Evaluating the importance of different coupled thermal, hydraulic, mechanical, and chemical process simulations during fluid flow experiments in fractured novaculite and fractured granite

Evaluating the importance of different coupled thermal, hydraulic, mechanical, and chemical process simulations during fluid flow experiments in fractured novaculite and fractured granite.

[1]Neil Chittenden, [2]Christopher McDermott, [1]Alexander Bond, [1]James Wilson, [3]Simon Norris

1 Quintessa Ltd, Henley-on-Thames and Warrington, UK
2 University of Edinburgh, School of Geoscience, Edinburgh, UK
3 Radioactive Waste Management Limited (RWM), UK

Abstract

Fluid migration in the subsurface has the potential to induce changes in fluid pressure distribution, temperature distribution, mechanical stresses and the chemistry of both the fluid and the natural geological material it is flowing through. In many situations, the change in all of these processes gives a coupled response, in that one process feeds back to another. When trying to understand fluid flow through naturally and artificially fractured systems, it is important to be able to identify the relative importance of the processes occurring and the degree of interactions between them. Modelling of such highly non-linear coupled flow is complex. Current and predicted computational ability is not able to simulate discretely all the known and physically described processes operating. One approach to coping with this complexity is to identify the relative importance and impact of relevant processes, dependent on the application of interest. Addressing such complexity can be particularly important when the characteristics of natural and disturbed geological materials are being evaluated in the context of disposal of radioactive waste or other geo-engineering systems where an understanding of the long-term evolution is required. Based on a series of coupled (THMC – Thermal, Hydraulic, Mechanical and Chemical) experimental investigations on the flow of fluid through fractured novaculite and granite crystalline rock samples, several couplings are examined where there is both a significant kinetic chemical control as well as mechanical and temperature control on the fluid flow behaviour. These interactions can be shown both in the literature and experimentally to have a significant effect on the rate of fluid flow through fractures. A new discrete numerical approach and a new homogenous approach are used to model the experimental results of coupled flow through fractures. The results of these modelling approaches are benchmarked both against one another and against the experimental results, and then the processes included in the approaches are ranked in order of impact.

Acknowledgements

This work was conducted within the international DECOVALEX Project (http://www.decovalex.org), with funding from Radioactive Waste Management Limited (RWM) (http://www.nda.gov.uk/rwm), a wholly–owned subsidiary of the Nuclear Decommissioning Authority.

1 Introduction

Fluid flow through fractured geological media has the potential to impact on the geological environment, e.g. (Garven *et al.* 2010, Goodwin *et al.* 2013, Harlov and Austrheim 2013 and references therein). When considering a Geological Disposal Facility (GDF) in a fractured host rock, it is necessary to demonstrate a sufficient understanding of fluid flow behaviour through the rock under relevant chemical (C), hydraulic (H), thermal (T) and mechanical (M) conditions. How fractures (either natural or induced by the construction process) evolve can affect re-saturation of a GDF, the local geochemical conditions, local connectivity and permeability, and hence impact the performance of the GDF, e.g. Bernier *et al.* (2007), Bond *et al.* (2010). Such fracture evolution can also be of significance for a range of other geo-engineering applications.

The evolution of fracture permeability, through interactions of mechanical and chemical processes under in situ stress affecting fracture aperture, is important in determining the fluid flow behaviour in fractured rock. Attempts at modelling fully-coupled THMC systems even on a single fracture have been limited, because the THMC processes occur at different physical scales and rates; this gives rise to numerical complexities in attempting to couple the solution of the energy or mass balance equations. Models calculating full numerical solutions of such systems are often complex and time consuming to run and require intricate numerical control to maintain stability in the solution. (e.g. Ouyang and Tamma, 1996; Kolditz, 1997; Wang *et al.*, 2011a; Wang *et al.*, 2011b)

This paper presents work carried out as part of Task C1 of the DECOVALEX 2015 project (DEvelopment of COupled models and their VALidation against EXperiments, www.decovalex.org), which has the objective of using the experimental data of Yasuhara *et al.* (2006 and 2011) to model the evolution of single novaculite and granite fractures through coupled THMC effects. Central to this task was building an understanding of the key physical processes in such a system from the available experimental data; understanding how such processes can be represented through numerical and/or semi-analytical models; and ranking the importance of these processes on the overall flow behaviour.

The work that is presented herein details the modelling in relation to the granite experiment (Yasuhara *et al.*, 2011) and builds on the earlier novaculite modelling work set out in Bond *et al.* (2014a, 2015) and McDermott *et al.* (2015), where discretised and homogenised models have been developed and tested at different scales and spatial resolutions. There is added complexity and associated uncertainty to the models in comparison to the novaculite experiment, in having to consider the different constituent minerals of the granite sample as opposed to a simple quartz chemistry for the novaculite. In order to capture the current understanding for modelling THMC behaviour in flow through a fracture, the importance of the processes included in the simulations and the associated uncertainties are then summarised.

The key processes identified in the novaculite modelling were mechanical closure of the fracture (pressure solution and/or stress corrosion); kinetically controlled mineral dissolution from the fracture surface; and development of preferential flow paths along the fracture surface, referred to as channel flow. Figure 1 from McDermott *et al.* (2015) illustrates the dominant effect of the different processes operating though the duration of the novaculite experiment. The geometry of the fracture was identified as a main controlling factor underpinning the key processes. Since accurate fracture aperture data are either not available or difficult to reconcile from surface scans, even from the accurate surface topography data available for the novaculite experiment, it must be approximated. It is represented in the discrete model using a high-resolution representation of the fracture geometry, and in the homogenised model using an upscaled single-box approach in which

the geometry is represented through an aperture-contact ratio relationship. The use of both discrete and homogenised models illustrate that there is considerable uncertainty in the aperture closure process and further uncertainty over the physical meaning of the large surface 'roughness' factor used to enhance dissolution from the fracture surface. Both pressure solution and stress corrosion are identified as important aperture closure processes in the literature, however the models highlighted that there was not enough information available to distinguish between pressure solution and stress corrosion as the aperture closure mechanism.

The focus of this paper is on the modelling of the granite experiment. The discrete and homogenised modelling approaches are further developed and applied using the new parameterisation. In particular, the homogenised model uses a full geochemical model to handle the chemistry of the different granite minerals and the poly-mineral pressure solution model from Yasuhara *et al.* (2011). The discrete model assumes that the quartz part of the granite is the controlling mineral for pressure solution and chemical dissolution, and uses an inverse chemistry modelling approach to fit the effluent ion concentrations giving further insight into the uncertainty associated with the chemical dissolution / granite mineral composition.

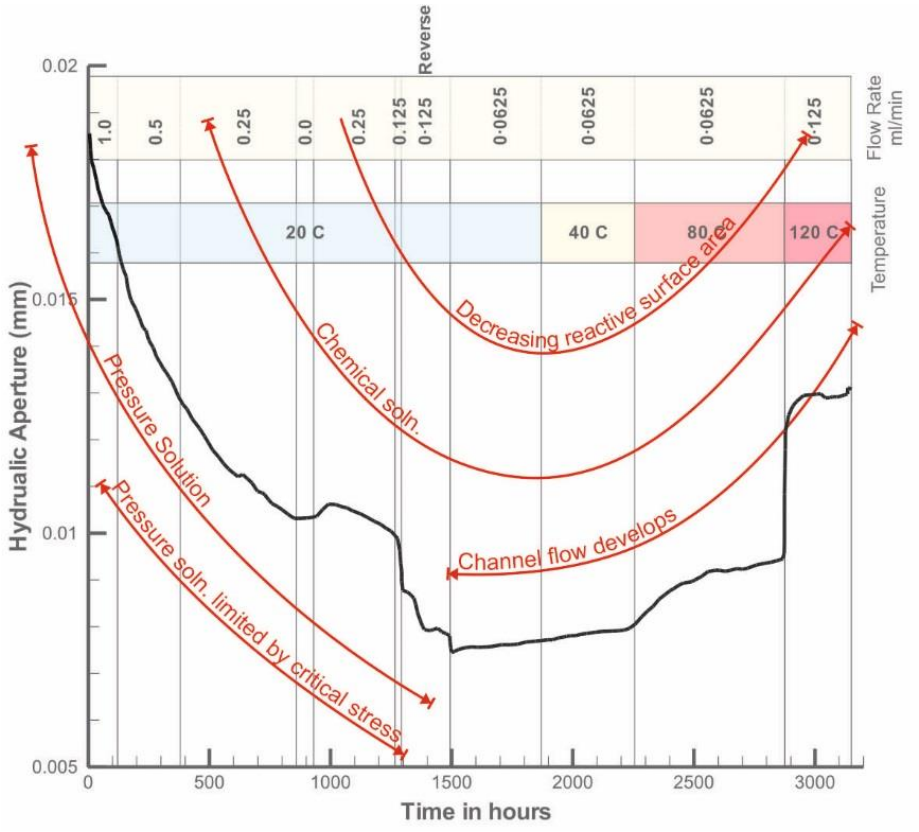

Figure 1: Suggestion of relative process importance in a pressure solution dominated system (for modelling of Yasuhara *et al.*, 2006, novaculite experiment) from McDermott *et al.* (2015).

2 Experimental data

Experiments were carried out by Yasuhara *et al.* (2011) to investigate the THMC evolution of three artificially fractured cylindrical samples of Mizunami granite (30 mm diameter × 60 mm length; single fracture as shown in Figure 2). The fracture was subject to the following conditions and measurements:

1. Hydraulic isolation and variable flow rates of de-ionised water across the fracture.
2. Mechanical confinement through the application of a confining pressure between 5 and 10 MPa.
3. Heating of the whole sample to different temperatures with time (Table 1).
4. Measurement of the major ion composition of the outflow and inflow and pH.
5. Measurement of differential pressures across the sample (Table 1).
6. Post-experiment inspection of the fracture surfaces using Scanning Electron Microscopy (SEM).

A schematic of the experiment is shown in Figure 2. Table 1 lists the key timings, temperatures and differential pressures used in the experiments. The timings for the change in differential pressure from 0.04 MPa to 0.1 MPa for samples ef-2 and ef-3 are stated in Yasuhara *et al.* (2011) as 477 hrs and 533 hrs, respectively. Through further internal communications during the course of this study, updated experimental information was provided; sample ef1 was 41.2 mm long (not 60 mm) and sample ef2 ran with an initial differential pressure of 0.1 MPa until 185 hrs before the 0.04 MPa period started.

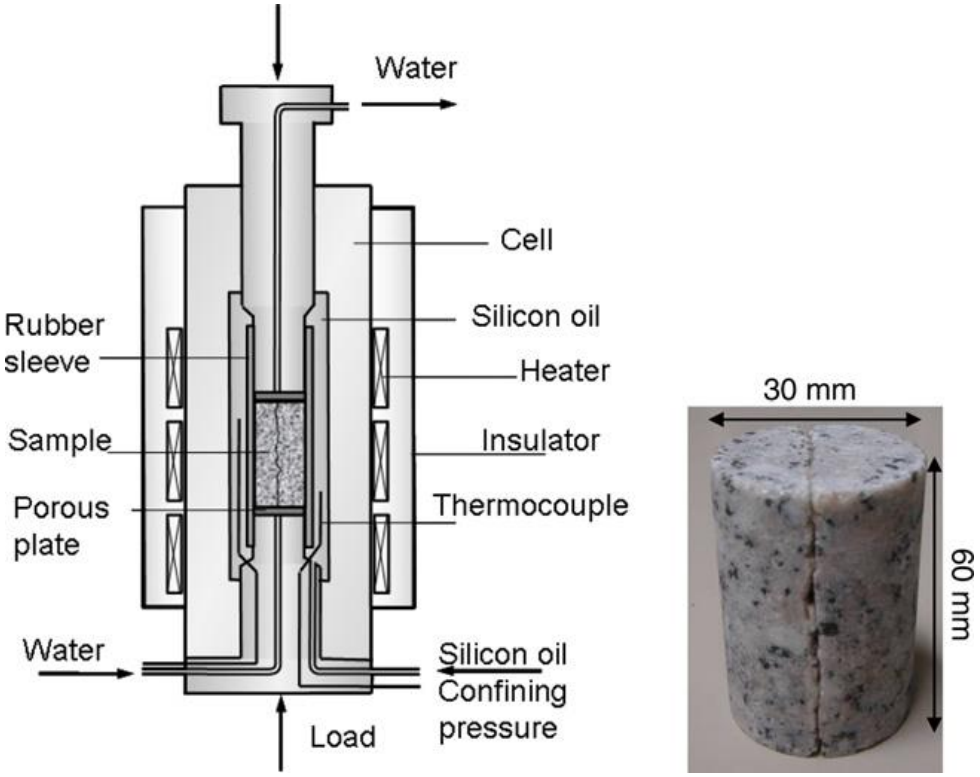

Figure 2: Experiment schematic (left) and one of the fractured samples (right) from Yasuhara *et al.* (2011)

Table 1: Key timings, temperatures and differential pressures for the three granite samples from Yasuhara *et al.* (2011). (* Internal communications with authors during the course of this study revealed that experiment ef-2 actually ran with an initial differential pressure of 0.1 MPa until 185 hrs before the 0.04 MPa period started.)

Sample	Confining Pressure (MPa)	Time (hr)	Thermal (°C)	Differential Pressure (MPa)
ef1	10	0-210 210-510	20 90	0.5
ef2	5	0-380 380-760	25 90	0.04-0.1 *
ef3	5	0-380 380-880	25 90	0.04-0.1

The evolution of major ion concentrations in the effluent and the water flow rate for the granite samples are shown in Figure 3 and Figure 4, respectively. The measured ion concentrations for samples ef-2 and ef-3 exhibit increases in concentration when the temperature is increased. Increase in concentration is also visible for sample ef-1 for Si and Mg; this observation is not as clear for the other major ions, which show large fluctuations in the experiment data. The flow rates show clear effects of the changes in temperatures and pressure during the experiments caused by change in water viscosity and fluid driving force, respectively. Furthermore, these experiments differ from the novaculite experiment (Yasuhara *et al.*, 2006) in only exhibiting an asymptotic decrease in flow rate over time, having no increase in effective fracture transmissivity apart from those associated with temperature and pressure discussed above.

The three rock samples were taken from Mizunami granite, however the granite mineralogy assumed by Yasuhara *et al.* (2011) for analysis appeared to be different from other published mineralogies for this granite; shown in Table 2. The 'alternative' composition is based on modal analyses reported in JNC (2000) and normative analysis performed using oxide data from Yuguchi *et al.* (2010), and is described in more detail in Bond *et al.* (2016a).

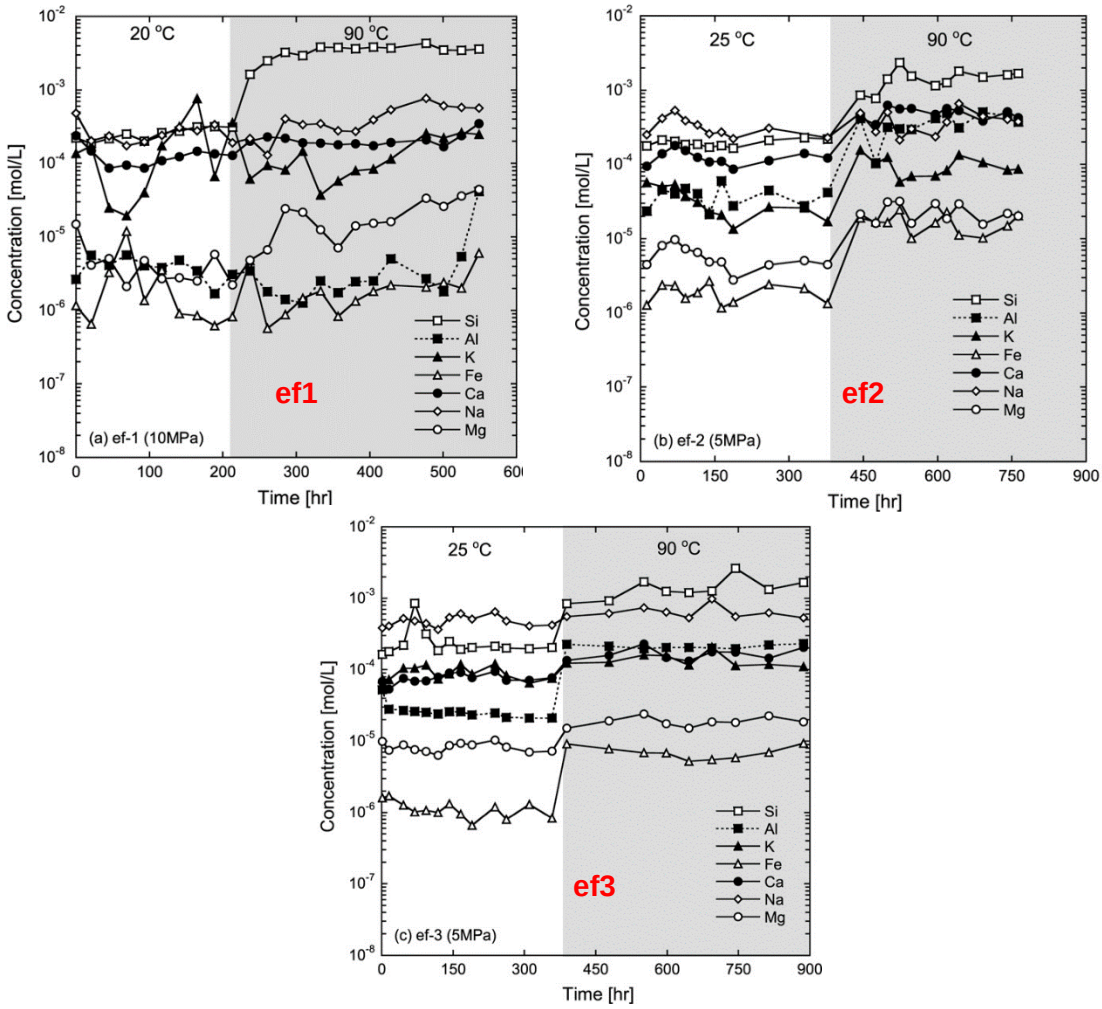

Figure 3: Major ion concentrations in experimental effluent for the three granite samples (from Yasuhara *et al.*, 2011). Temperature changes during the experiment are shown on the graphs.

ef1

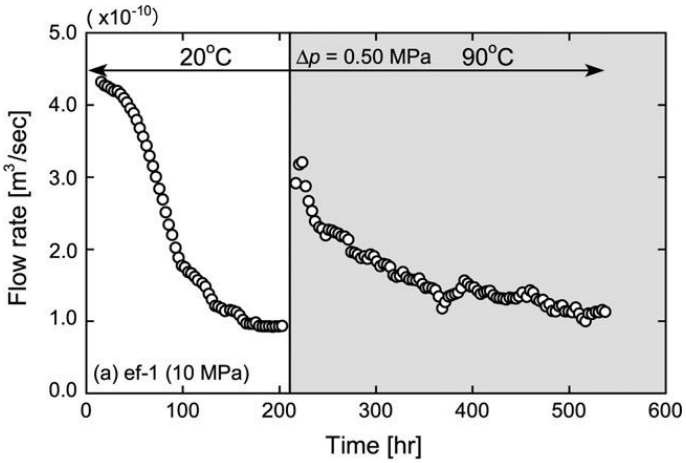

ef2

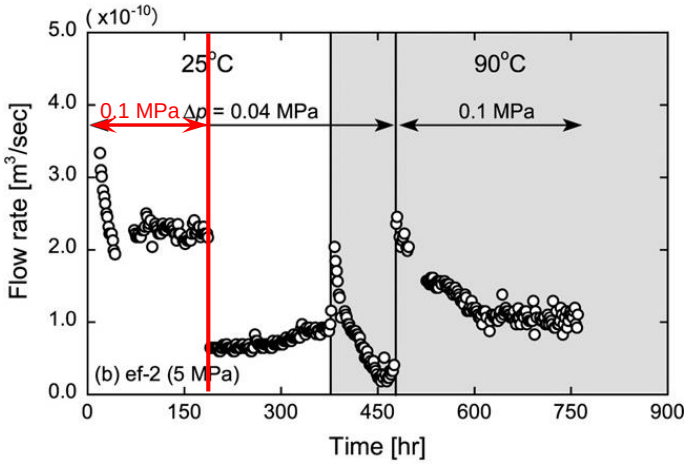

ef3

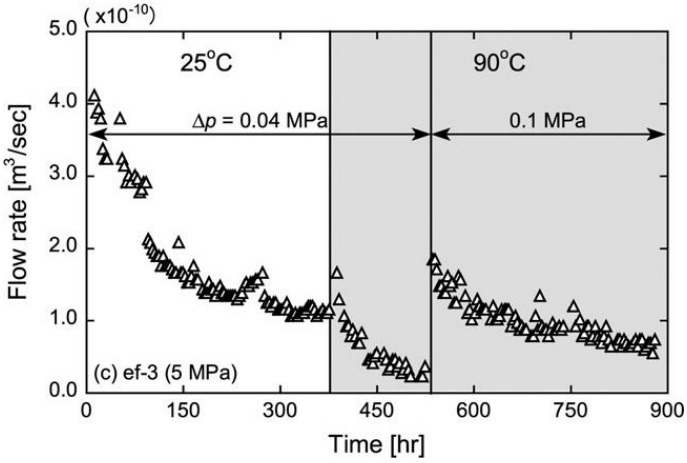

Figure 4: Flow rates for the three granite samples (from Yasuhara *et al.*, 2011). Temperature and pressure changes during the experiment are shown on the graphs. For ef2, the initial differential pressure of 0.1 MPa until 185 hrs before the 0.04 MPa period started has been marked (red).

Table 2: Simplified Toki granite composition from Yasuhara *et al.* (2011) and an 'alternative' composition based on modal analyses reported in JNC (2000) and normative analysis performed using oxide data from Yuguchi *et al.*, (2010).

Mineral	**Idealised Composition**	**V_{min} (cc/mol)**	**Yasuhara**	**Alternative**	
			vol%	wt%	vol%
Quartz (Q)	SiO_2	22.688	50	33	32.99
K-feldspar (orthoclase)	$KAlSi_3O_8$	108.87	25	25	25.89
Plagioclase (albite)	$NaAlSi_3O_8$	100.25	10	32	32.38
Plagioclase (anorthite)	$CaAl_2(SiO_4)_2$	100.79	10	4	3.84
Biotite (annite)	$KFe_3AlSi_3O_{10}(OH)_2$	154.32	5	5.2	4.15
Biotite (phlogopite)	$KMg_3AlSi_3O_{10}(OH)_2$	149.66	None	0.8	0.76
Total			**100**	**100**	**100**

3 Models

Modelling of the Yasuhara *et al*. (2006) novaculite experiment (Bond *et al.*, 2014a, 2015; McDermott *et al.*, 2015) identified the key processes as mechanical closure of the fracture (pressure solution and/or stress corrosion), kinetically controlled mineral dissolution from the fracture surface, and development of channel flow (discrete model) – all of which are underpinned by choice of aperture distribution. For the granite study, these are all again considered to be important, as well as the further complexity and associated uncertainty in having to consider the different minerals that make up the sample (in contrast to the simple quartz chemistry of the novaculite). Both the discretised and homogenised modelling approaches have been developed and applied to the granite experiments.

The discretised model works by generating a fracture aperture map at the desired scale of interest and then simulating flow, transport and aperture mechanics on a finite element grid (Bond *et al.*, 2015; McDermott *et al.*, 2015) using the OpenGeoSys (OGS; Kolditz *et al.*, 2016) code. McDermott *et al.* (2015) discuss the numerical techniques adopted to allow the representation of rapid mechanical and chemical processes at small scales on relatively coarse grids to generate the fracture closure and then opening seen in the experimental data (Figure 1). This included the use of streamline dissolution to create the channelization effects seen in the high temperature novaculite data. That said, due to the complexity and added uncertainties for modelling the different minerals within the granite, as well as the trend of closing hydraulic aperture across the experiment for the three granite samples, channel development is not considered in the granite model. This is reasonable since channel development was shown to be an important process in limiting fracture opening in the novaculite modelling, which is not observed in the granite samples used in this study. Furthermore, instead of a full geochemical model, the discrete model applies a simplified geochemical model where quartz is assumed to control aperture closure and the effluent ion concentrations from the other minerals using an inverse chemistry modelling approach. This allows the discretised model to be applied to the granite experiment without significant extra complexity over the model of the novaculite experiment. Quartz controlling the aperture closure is a reasonable assumption since it is not a very reactive mineral and is most prevalent within the granite.

The homogenised model for granite builds on the previous novaculite experiment modelling work detailed in Bond *et al.* (2014a, 2015), implemented using the Quintessa multi-physics code QPAC (Maul, 2013; Bond *et al.*, 2013; Benbow *et al.*, 2014). By representing the fracture at a coarse, even single box, resolution, the more complex chemistry for granite can be introduced, keeping a fully-coupled system without significant extra computation overhead. This allows the importance of the geochemical dissolution/precipitation processes to be investigated within the context of this study. A schematic illustration of the flow through the fracture and the coupling for the granite homogenised model is shown in Figure 5. The fracture through which fluid can flow is represented through the open volume of a single box granite compartment whereby the coupled processes of chemical dissolution (reactive transport) at the fracture walls and mechanical dissolution (pressure solution) at touching asperities under stress act to open / close the open volume. Thus, affecting the average hydraulic conductivity of the fracture. The touching asperities are represented through an aperture-contact ratio relationship in which a representative summed area of the local asperity contacts can be determined from the current aperture.

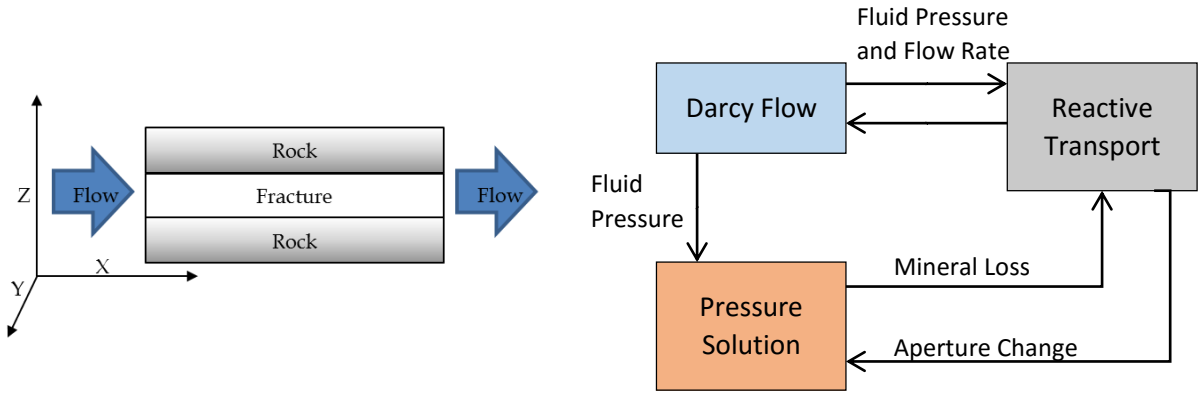

Figure 5: Schematic illustration of the flow through the fracture (left) and coupling (right) in the QPAC homogenised model

Applying both the discretised model and the homogenised model to the granite experiment enables investigation and comparison of the different processes that they can represent at different scales. The discretised model uses a high-resolution grid to represent the fracture to model small-scale features from flow across the fracture surface and, in particular, the evolving aperture-contact ratio relationship, but is limited to simple chemistry calculation. The homogenised model applies an upscaled approach with full process coupling, fully representing the complex granite geochemistry. However, it does not represent the small-scale features across the fracture surface and relies on a predetermined aperture-contact ratio relationship.

The key model components of the aperture distribution, the mechanical closure process, and the mineral dissolution process, are discussed in greater detail below. The development of the discrete and homogenised modelling approaches, including some further technical details of the models, is available in the peer-reviewed, online-accessible technical reports Bond *et al.* (2014a, 2015, 2016a, 2016c).

3.1 Aperture distribution

The fracture topography is important as it is a key underpinning aspect of the different processes within the model, both in terms of the reactive surface area for the chemical dissolution process and the stress concentration controlling the mechanical closure of the fracture. In order to model

processes in an internally-consistent manor, it is important to have a representative surface of the fracture for the relevant scale of processes. For the discrete model, this is achieved using an aperture distribution, and for the homogenised model this is done using a modified aperture-contact ratio distribution based on the relationship given in Yasuhara *et al.* (2006) and cross-checked for consistency against the discretised distribution.

The complete fracture surface topography data available for the novaculite experiment (Yasuhara *et al.*, 2006) is a type of dataset that is not typically available for use in modelling flow through fractures in rock. Indeed, for the granite experiment (Yasuhara *et al.*, 2011), no such data are available. Even with surface topography data for either side of a fracture, difficulties can arise on attempting to directly construct an aperture profile using this data, as discussed in Bond *et al.* (2015). As such, for discretised models of a fracture it becomes necessary to use a synthetic topography which can be generated through statistical methods based on analysis of representative generic fractures. In this study, the asperity data from the novaculite experiment is considered to be representative fracture surface data, from which an aperture distribution can be derived for the granite experiment.

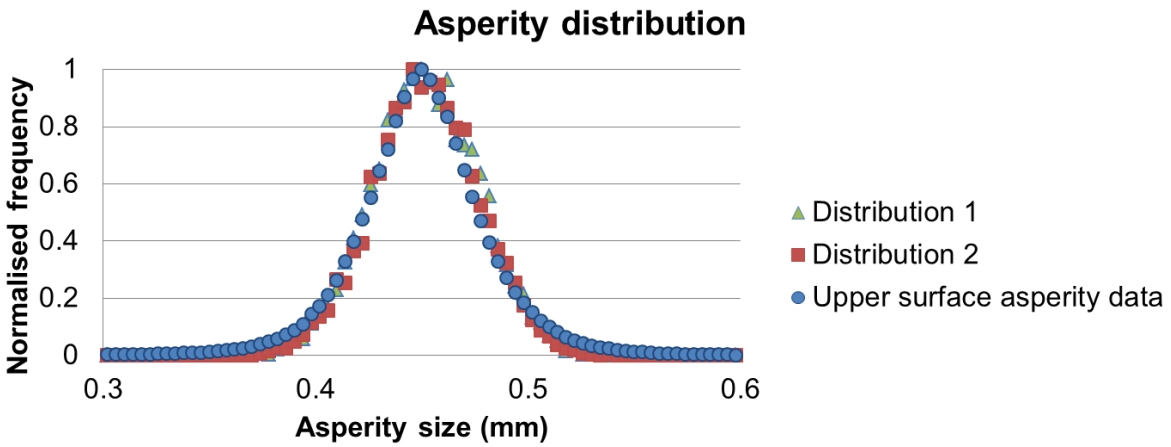

Figure 6: High resolution asperity surface distribution, and two statistically identical generated profiles (Distribution 1 and 2) fitting the novaculite experiment surface profile data, where the mean value is 0.45 mm and the standard deviation is 0.025 mm from Bond *et al.* (2016a)

For generating the synthetic aperture data, two normal distributions (X_1, X_2) are fitted to the asperity data from the novaculite experiment (Figure 6), described mathematically in (1), where μ is the mean (mm) and σ is the standard deviation (mm).

$$X_1 = N(\mu, \sigma^2)$$
$$X_2 = N(\mu, \sigma^2) \quad (1)$$

Equation (2) shows how the aperture is then evaluated by combining these two asperity distributions, where e_0 can be considered to be the average fracture aperture, and m is the mismatch parameter between the two surfaces. The selection of the values for e_0 and m to represent the novaculite aperture data are described in detail in Bond *et al.* (2016a).

$$e = e_0 + m(X_1 - X_2) \quad (2)$$

The discretised model uses this same basic distribution derived from the novaculite data but then calibrated to the granite experiments (Bond *et al.*, 2016a) using the parameters shown in Table 3. The authors recognise that there are uncertainties in the aperture distribution, and that this is one particular representation of the fracture aperture for the granite samples. By fixing the aperture distribution in this way in the initial conditions, the effect of the different processes can still be

investigated for this study. The model results herein are based on this assumption for the initial condition.

Table 3: Aperture distribution parameters calibrated to the granite experiments

Sample	e_0 (m)	m	Minimum aperture (m)	Mean, μ	Standard deviation, σ
ef1	0.0025 mm	0.03	6.00E-07	0.0025 mm	0.0055 mm
ef2	0.0055 mm	0.066	1.00E-06		
ef3	0.006 mm	0.08	1.50E-06		

The homogenised model of the granite experiment uses a simple contact ratio-aperture model as used in the novaculite modelling, shown in (3), where b_r is the residual aperture (m), b_0 is the initial aperture (m), R_c is the contact ratio (-), R_{c0} is the initial contact ratio (-), and a is a fitting parameter (-).

$$b = b_r + (b_0 - b_r)\exp\left(-\frac{R_c - R_{c0}}{a}\right) \quad (3)$$

The parameters used for the aperture-contact ratio relationship for modelling the granite experiment ef3 are shown in Table 4.

Table 4: Parameters for homogenised model aperture-contact ratio relationship

R_{c0} (-)	0.025
a (-)	0.04 (Fig. 11, Yasuhara *et al.*, 2011)
b_r	0.4 µm
b_0	6 µm

3.2 Mechanical closure

The mechanical dissolution process (pressure solution / stress corrosion) is considered to be the dominant process affecting fracture aperture closure in the granite experiment. Details of how this process is represented within the discretised and homogenised models are presented below.

3.2.1 Discretised model

For the discretised model (McDermott *et al.*, 2015), the hydraulic system is solved numerically, and analytical and physical models are used to include mechanical deformation, pressure solution and chemical dissolution processes as a function of the hydraulic properties. This is illustrated in Figure 7 from McDermott *et al.* (2015). The mechanical closure is calculated within the time step solve using a series of explicit iterations converging on the solution for closure during this time step. It does this by evaluating the stress dependent closure for a given number of contacts (evaluated from competing pressure solution and surface dissolution processes) and calculates the resulting increase in contacts per iteration, bisecting on the number of contacts until this value no longer increases.

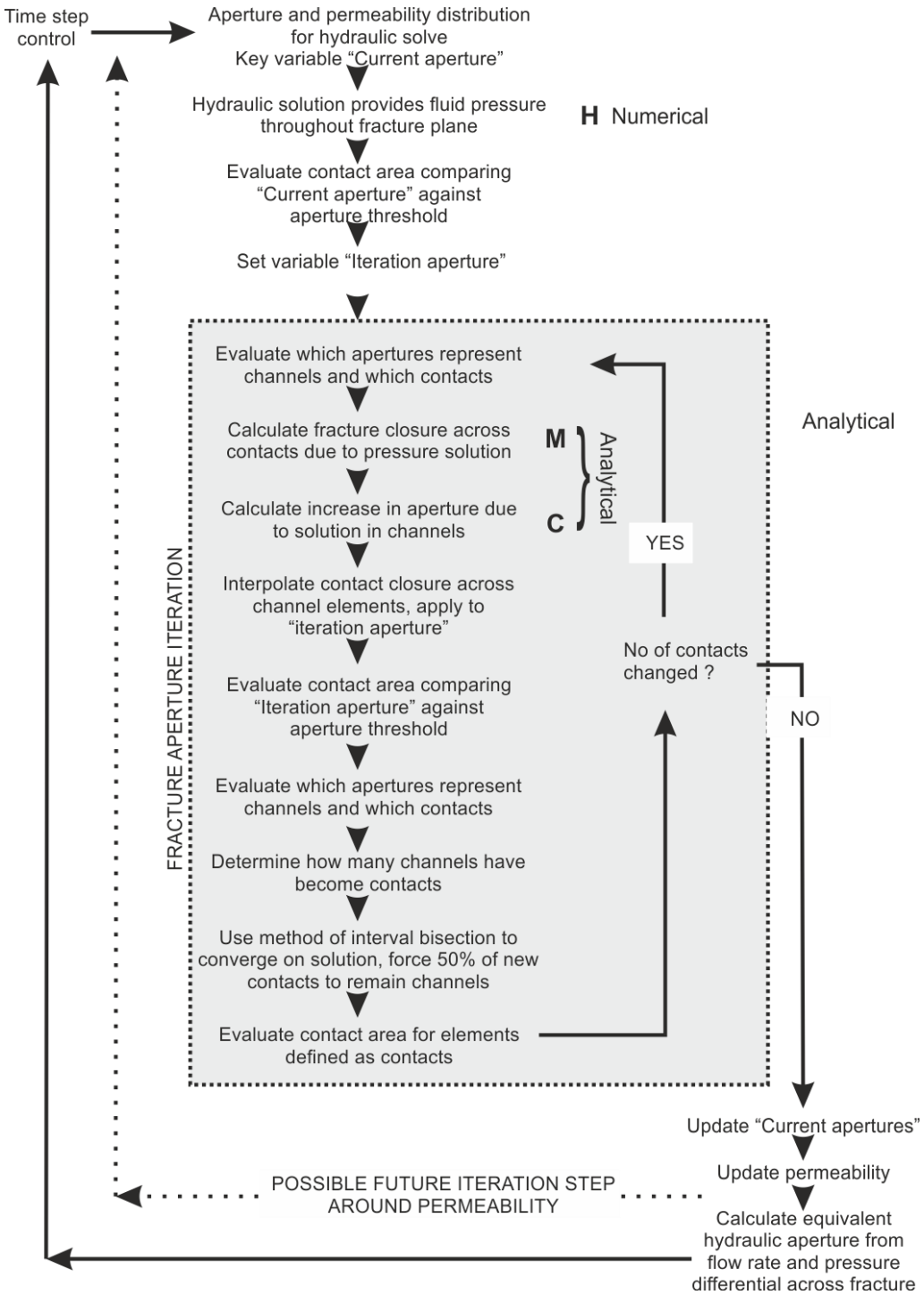

Figure 7: Implementation of the H(MC) application for fracture aperture alteration in the discretised model from McDermott *et al.* (2015)

3.2.2 Homogenised model

The homogenised model applies the poly-mineral pressure solution model from Yasuhara *et al.* (2011), shown in (4), to calculate a predicted rate of mineral dissolution due to pressure solution,

$$\dot{M}_{diss,i}^{PS} = f_{r,i} x_i^V \frac{3V_{m,i}^2(\sigma_a - \sigma_c)k_{+,i}\rho_{g,i}A_c}{RT} \quad (4)$$

$$f_{r,i} = \frac{S_{BET,i} d_i \rho_{g,i}}{6}$$

$$k_{+,i} = k^0_{+,i} e^{-\frac{E_{a_i}}{RT}}$$

where for mineral i, $\dot{M}^{PS}_{diss,i}$ is the rate of dissolution (kg s^{-1}), $f_{r,i}$ is the roughness factor (-), x^V_i is the volumetric ratio of mineral i (-), $V_{m,i}$ is the molar volume of mineral i (m^3 mol^{-1}) , σ_a is the effective stress (Pa), σ_c is the critical stress (Pa), $k_{+,i}$ is the dissolution rate constant for pressure solution (mol m^{-2} s^{-1}), $\rho_{g,i}$ is the density of mineral i (kg m^{-3}), A_c is the size of local contact area (m^2), R is the gas constant (J K^{-1} mol^{-1}), T is the temperature (K), $S_{BET,i}$ is the specific surface area (m^2 kg^{-1}), d_i is the grain diameter (m), $k^0_{+,i}$ is a pre-exponential factor for the rate constant (mol m^{-2} s^{-1}), and E_{a_i} is the activation energy for rate constant (J mol^{-1}). Key parameters are given in Table 5.

Table 5: Pressure solution parameters (Yasuhara *et al.*, 2011)

Parameter	Description	Value	Unit
$\dot{M}^{PS}_{diss,i}$	Rate of dissolution		kg s^{-1}
$f_{r,i}$	Roughness factor	$\frac{S_{BET,i} d_i \rho_{g,i}}{6}$	-
x^V_i	Volumetric ratio of mineral i	From model (vol. %)	-
$V_{m,i}$	Molar volume of mineral i	From QPAC Reactive Transport Module	m^3 mol^{-1}
σ_a	Effective stress	$\sigma_a = \sigma - \sigma_w$ $\sigma = 5$ MPa	Pa
σ_c	Critical stress	100	MPa
$k_{+,i}$	Dissolution rate constant for pressure solution	$k^0_{+,i} e^{-\frac{E_{a_i}}{RT}}$	mol m^{-2} s^{-1}
$\rho_{g,i}$	Density of mineral i	From QPAC Reactive Transport Module	kg m^{-3}
A_c	Local contact area	From contact-ratio aperture relationship	m^2
$S_{BET,i}$	Specific surface area	0.51	m^2 g^{-1}
d_i	Grain diameter	178	µm
$k^0_{+,i}$	Pre-exponential factor for rate constant	Table 4 (Yasuhara *et al.*, 2011)	mol m^{-2} s^{-1}
E_{a_i}	Activation energy	Table 4 (Yasuhara *et al.*, 2011)	J mol^{-1}

The per-mineral pressure solution rates can then be used to calculate a volumetric dissolution rate from pressure solution over the contacting area. As for the previous homogenised model of the novaculite (Bond *et al.*, 2015), this closure is then represented through adding volume to the porosity over the entire fracture surface area as shown in Figure 8.

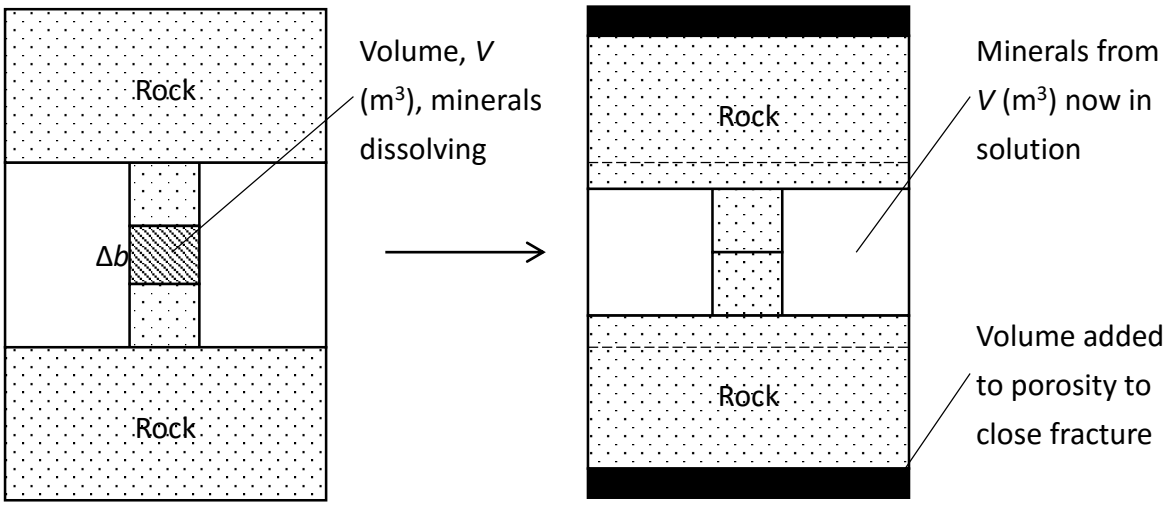

Figure 8: Diagram of mechanical closure represented through porosity change for the homogenised model

3.3 Chemical dissolution

Surface dissolution (and precipitation) of the constituent minerals of the granite is a significant process which affects effluent ion concentration. This is calculated in the homogenised model with a full geochemical model of the complex granite chemistry. The discretised model uses a simplified inverse geochemical model derived from the dissolved quartz concentration. Details of these models are presented below.

3.3.1 Full geochemical model

The kinetically-controlled mineral dissolution/precipitation reactions use a routinely-applied Transition State Theory (TST)-based approach represented by (Aagaard and Helgeson, 1982; Palandri and Kharaka, 2004; *inter alia*):

$$\frac{dS}{dt} = A(S)(k_1 a_H^{n1} + k_2 + k_3 a_H^{n3} + k_4 f_{CO2}^{n4})\left(\frac{Q}{K} - 1\right) \quad (5)$$

where S (mol) is the abundance of the solid of interest, t is time (s), $k_{1,2,3,4}$ are the rate constants (mol/(m^2 s)) for acid, neutral, base and carbonate mechanisms, $A(S)$ is the mineral reactive surface area (m^2) (which is a function of the mineral abundance), n is a dimensionless catalysis constant for acid- (n_1), base- (n_3) and carbonate- (n_4) dependent rates, Q is the ion activity product, a_{H+} is the activity of the hydrogen ion, f_{CO_2} is the CO_2 fugacity, and K is the equilibrium constant for mineral dissolution. Except for surface area and k, these terms are dimensionless.

To model the mineral dissolution/precipitation at the different temperatures used in the experiment, reaction rates are calculated from an Arrhenius relationship (6) of activation energy to reaction rate using reference measured reaction rates at 25 °C.

$$k_i = k_i^{(25)} e^{\frac{E_{a_i}}{R}\left(\frac{1}{T_{25}} - \frac{1}{T}\right)} \quad (6)$$

Here, E_{a_i} is the activation energy for the reaction of interest (J/mol), R is the gas constant (J K^{-1} mol^{-1}), T is the temperature (K), and $k_i^{(25)}$ and T_{25} are the reaction rate (mol/(m^2 s)) and temperature (K) at 25 °C, respectively, which relate the calculated reaction rate to the reference measured reaction rate.

Updating (5) with (6), gives:

$$\frac{dS}{dt} = A(S)\left(\begin{array}{l} k_1^{(25)} e^{\frac{E_{a_1}}{R}\left(\frac{1}{T_{25}}-\frac{1}{T}\right)} a_H^{n1} + k_2^{(25)} e^{\frac{E_{a_2}}{R}\left(\frac{1}{T_{25}}-\frac{1}{T}\right)} + \\ k_3^{(25)} e^{\frac{E_{a_3}}{R}\left(\frac{1}{T_{25}}-\frac{1}{T}\right)} a_H^{n3} + k_4^{(25)} e^{\frac{E_{a_4}}{R}\left(\frac{1}{T_{25}}-\frac{1}{T}\right)} f_{CO2}^{n4} \end{array} \right)\left(\frac{Q}{K} - 1\right) \qquad (7)$$

The values of equilibrium constants and kinetic parameters in (7) for the different reactions considered for the granite are summarised below. Equilibrium constants (log *K* values; Table 6 and Table 7) are taken from the Geochemist's Workbench® (GWB; Bethke, 2008) database thermo.com.v8.r6+ and, where data were not available for T ≠ 25°C, from the thermoddem (v1.07; BRGM, 2011) and thermochimie (v9; Andra, 2014) databases. Log *K* values for the experiment temperatures are interpolated from the available standard temperature values. Kinetic data (Table 8 and Table 9) for the dissolution and precipitation of primary/secondary minerals are taken from Palandri and Kharaka (2004). Full detail of the thermodynamic data used and how the aqueous species present in the geochemical model were identified can be found in Bond *et al.* (2016a).

Table 6: Equilibrium constants for mineral hydrolysis reactions (taken from Geochemist's Workbench database thermo.com.v8.r6+).

Mineral	Hydrolysis Reaction	log *K* 0°C	log *K* 25°C	log *K* 60°C	log *K* 100°C
Primary Minerals					
Quartz	$SiO_{2(s)} = SiO_{2(aq)}$	-4.6319	-3.9993	-3.4734	-3.0782
Annite	$Kfe_3AlSi_3O_{10}(OH)_2 + 10H^+ = Al^{3+} + K^+ + 3Fe^{2+} + 3SiO_{2(aq)} + 6H_2O$	33.3018	29.4693	24.4456	19.6118
Phlogopite	$KMg_3AlSi_3O_{10}(OH)_2 + 10H+ = Al^{3+} + K^+ + 3Mg^{2+} + 3SiO_{2(aq)} + 6H_2O$	42.0937	37.44	31.5103	25.9003
Albite	$NaAlSi_3O_8 + 4H^+ = Al^{3+} + Na^+ + SiO_{2(aq)} + H_2O$	3.273	2.7645	1.5678	0.2236
Anorthite	$CaAl_2(SiO_4)2 + 8H^+ = Ca^{2+} + 2Al3+ + 2SiO_{2(aq)} + 4\ H_2O$	31.1921	26.578	20.809	15.3121
K-Feldspar	$KalSi_3O_8 + 4H^+ = Al^{3+} + K^+ + 3SiO_{2(aq)} + 2H_2O$	-0.2168	-0.2753	-0.961	-1.8555
Secondary Minerals					
amorphous silica	$SiO_{2(s)} = SiO_{2(aq)}$	-3.124	-2.7136	-2.4067	-2.1843
chalcedony	$SiO_{2(s)} = SiO_{2(aq)}$	-4.3359	-3.7281	-3.2307	-2.8615
calcite	$CaCO_3 + H^+ = Ca^{2+} + HCO_3^-$	2.2257	1.8487	1.333	0.7743

Table 7: Equilibrium constants for reactions between basis and secondary aqueous species. Values in italics were taken from thermoddem (v1.07; BRGM, 2011) and were used in reactive transport models when data were not included in the GWB database at T ≠ 25ºC.

Species	Reaction	log *K* 0°C	log *K* 25°C	log *K* 60°C	log *K* 100°C
AlO_2-	$AlO_2^- + 4H^+ = Al^{3+} + 2H_2O$	25.7948	22.8833	19.5707	16.5819
$HalO_{2(aq)}$	$HalO_{2(aq)} + 3H^+ = Al^{3+} + 2H_2O$	18.7152	18.7152	13.7251	11.1731
$Al(OH)_2^+$	$Al(OH)_2^+ + 2H^+ = A^{l3+} + 2H_2O$	12.1394	10.5945	8.7455	6.9818
$NaAlO_{2(aq)}$	$NaAlO_{2(aq)} + 4H^+ = Al^{3+} + Na^+ + 2H_2O$	26.6454	23.6266	20.0941	16.8223
$FeOH^+$ (GWB)[1]	$FeOH^+ + H^+ = Fe^{2+} + H_2O$	-	9.5	-	-
$FeOH^+$ (TD)[2]	*$FeOH^+ + H+ = Fe^{2+} + H_2O$*	*10.3808*	*9.501*	*8.4812*	*7.547*
$Fe(OH)_{3(aq)}$[3]	$Fe(OH)_{3(aq)} + 3H^+ = Fe^{3+} + 3H_2O$	13.7	12	10.1	8.3
$Fe(OH)_4^-$ (GWB)[1]	$Fe(OH)_4^- + 4H^+ = Fe^{3+} + 4H_2O$	-	21.6	-	-
$Fe(OH)_4^-$ (TD)[2]	*$Fe(OH)_4^- + 4H^+ = Fe^{3+} + 4H_2O$*	*23.9677*	*21.6041*	*18.9594*	*16.5536*
$NaHSiO_{3(aq)}$	$NaHSiO_{2(aq)} + H^+ = Na^+ + H_2O + SiO_{2(aq)}$	8.4138	8.304	8.053	7.8291
$HsiO_3^-$	$HsiO_3^- + H^+ = SiO_{2(aq)} + H_2O$	10.3231	9.9525	9.4684	9.0844
$CO_{2(aq)}$	$CO_{2(aq)} + H_2O = H^+ + HCO_3^-$	-6.5804	-6.3447	-6.2684	-6.3882
CO_3^{2-}	$CO_3^{2-} + H^+ = HCO_3^-$	10.6241	10.3288	10.1304	10.0836
$MgHCO_3^+$	$MgHCO_3^+ = HCO_3^- + Mg^{2+}$	-1.0798	-1.0357	-1.1638	-1.4355
$MgCO_{3(aq)}$	$MgCO_{3(aq)} + H^+ = HCO_3^- + Mg^{2+}$	7.7399	7.3499	6.9262	6.5632
$CaHCO_3^+$	$CaHCO_3^+ = Ca^{2+} + HCO_3^-$	-1.0951	-1.0467	-1.1592	-1.4181
$CaCO_{3(aq)}$	$CaCO_{3(aq)} + H = Ca^{2+} + HCO_3^-$	7.5021	7.0017	6.4516	5.9636
$FeHCO_3^+$ (GWB)[1]	$FeHCO_3^+ = Fe^{2+} + HCO_3^-$	-	-2.72	-	-
$FeHCO_3^+$ (TD)[2]	*$FeHCO_3^+ = Fe^{2+} + HCO_3^-$*	*-1.3976*	*-1.44*	*-1.5215*	*-1.6248*
$FeCO_{3(aq)}$ (GWB)[1]	$FeCO_{3(aq)} + H^+ = Fe^{2+} + HCO_3^-$	-	5.5988	-	-
$FeCO_{3(aq)}$ (TD)[2]	*$FeCO_{3(aq)} + H+ = Fe^{2+} + HCO_3^-$*	*4.7641*	*4.6367*	*4.4576*	*4.2652*
$NaHCO_{3(aq)}$	$NaHCO_{3(aq)} = HCO_3^- + Na^+$	-0.3734	-0.1541	0.1098	0.4108

1. Data from thermo.com.v8.r6+
2. Data from thermoddem (v1.07) (http://thermoddem.brgm.fr/)
3. log K values at T ≠ 25ºC approximated using the Van't Hoff equation and a value of ΔH_f of -103.764 kJ/mol from ThermoChimie (v9) (http://www.thermochimie-tdb.com/)

Table 8: Kinetic data for dissolution of primary and secondary minerals (from Palandri and Kharaka, 2004).

Mineral	Acid			Neutral		Base			Carbonate		
	log k_1	n_1	Ea_1	log k_2	Ea_2	log k_3	n_3	Ea_3	log k_4	n_4	Ea_4
	mol/m^2/s	-	kJ/mol	mol/m^2/s	kJ/mol	mol/m^2/s	-	kJ/mol	mol/m^2/s	-	kJ/mol
Primary Minerals											
quartz	-	-	-	-13.34	90.10	-	-	-	-	-	-
annite and phlogopite	-9.84	0.53	22.00	-12.55	22.00	-	-	-	-	-	-
albite	-10.16	0.46	65.00	-12.56	69.80	-15.60	0.57	71.00	-	-	-
anorthite	-3.50	1.41	16.60	-9.12	17.80	-	-	-	-	-	-
K-Feldspar	-10.06	0.50	51.70	-12.41	38.00	-21.20	0.82	94.10	-	-	-
Secondary Minerals											
amorphous silica/chalcedony	-	-	-	-12.77	68.70	-	-	-	-	-	-
calcite	-0.30	1.00	14.40	-5.81	23.50	-	-	-	-3.48	1.00	35.40

Table 9: Kinetic data for precipitation of amorphous silica/chalcedony (from Palandri and Kharaka, 2004).

Mineral	Acid			Neutral		Base			Carbonate		
	log k_1	$n1$	Ea_1	log k_2	Ea_2	log k_3	n_3	Ea_3	log k_4	n_4	Ea_4
	mol/m^2/s	-	kJ/mol	mol/m^2/s	kJ/mol	mol/m^2/s	-	kJ/mol	mol/m^2/s	-	kJ/mol
amorphous silica/chalcedony	-	-	-	-9.42	49.8	-	-	-	-	-	-

3.3.2 Inverse geochemical model

The discretised model uses a highly simplified inverse geochemical model where quartz is assumed to be the main control for aperture closure and loss of other minerals, and so the concentrations of ions in solution are fitted to back-calculate a mineralogy which can be compared back to the input granite mineralogy. This approach was preferred since implementing a full geochemical model into the discretised model would be extremely difficult and time consuming for extending the numerical techniques that were used for the novaculite model (Bond *et al.*, 2015; McDermott *et al.*, 2015) to the granite.

The volume change of the fracture surface through mineral dissolution between contact areas is calculated by the discretised model. This volume change is then interpreted based on the mineral composition of the granite to calculate ion concentrations from the non-quartz minerals and calibrated to the experiment concentration data. The assumed mineral composition of the granite is shown in Table 2 ('alternative' composition) with corresponding stoichiometry in Table 10.

Table 10: Stoichiometry

	Si^{4+}	Al^{3+}	K^{+}	Fe^{2+}	Ca^{2+}	Na^{+}	Mg^{+}	O^{2-}	OH^{-}
Quartz	1							2	
Anorthite	2	2			1			8	
Albite	3	1				1		8	
Orthoclase	3	1	1					8	
Phlogobite	3	1	1				3	10	2
Annite	3	1	1	3				10	2

From Table 10 the individual marker minerals responsible for the cation species in the effluent can be identified, as presented in Table 11. This table also presents the molar volume ratio, which is important as the volume of SiO_2 the numerical model predicts is related via the inverse model to the cation concentration.

Table 11: Elements which could only come from a particular mineral in the Granite

Measured cations	Mineral	Volume ratio
Ca^{2+}	Anorthite	4.44
Na^{+}	Albite	4.41
Fe^{3+}	Annite	6.79
Mg^{2+}	Phlogopite	6.59

The inverse model is described below, with the mathematical symbols summarised in Table 12.

Table 12: Table of symbols for geochemical inverse model

Symbol	Units	Description
C_{Si}^{chem}	mol/l	Concentration of Si from model (non Pressure Solution) in standard units
C_j	mol/l	Concentration of element j in mol/l

$f_Q, f_G, f_{Al(aq)}$	-	Volume fractions of solute, Q=quartz, G=granite (non-quartz), Al(aq)=aluminium, vals = 0.97, 0.03, 0.0040 respectively
R_{mol}^{j}	-	Mole ratio of element j
n_Q, n_G	mol/l	Moles quartz and granite dissolved
$V_{m,Q}, V_{m,G}$	cc/mol	Molar volume of quartz and granite

The discretised model predicts a volume change of the fracture surface as a consequence of mineral dissolution, giving a Si concentration C_{Si}^{chem}, which has components from quartz dissolution and granite dissolution:

$$C_{Si}^{chem} = n_Q + R_{mol}^{Si} n_G \tag{8}$$

For a given volume-concentration of solute, *V* (cc/l), we can write:

$$\begin{aligned} V_Q &= f_Q V = n_Q V_{m,Q} \\ V_G &= f_G V = n_G V_{m,G} \end{aligned} \tag{9}$$

Therefore,

$$n_Q = \frac{f_Q n_G V_{m,G}}{f_G V_{m,Q}} \tag{10}$$

Combining (10) and (8):

$$C_{Si}^{chem} = \left(\frac{f_Q V_{m,G}}{f_G V_{m,Q}} + R_{mol}^{Si} \right) n_G \tag{11}$$

This allows n_G, the number of moles of granite dissolved, to be calculated as:

$$n_G = \frac{C_{Si}^{chem}}{\left(\frac{f_Q V_{m,G}}{f_G V_{m,Q}} + R_{mol}^{Si} \right)} \tag{12}$$

Hence, using the element mole ratios for a given composition of the granite, this leads to the expression:

$$C_j = R_{mol}^{j} n_G \tag{13}$$

This is then used to evaluate the other effluent ion concentrations from C_{Si}^{chem}, calculated by the discretised model. That said, this approach leads to underestimating of the cation concentration for those other than Si due to two further processes; the kinetic rate of quartz dissolution is much slower than that of the other minerals present in granite, and; C_{Si}^{chem} only accounts for the volume change as a result of chemical dissolution on the fracture walls and does not include fluid interactions from the matrix where ions can diffuse from within the fracture surface. With these processes, C_j will tend to be larger.

Equation (13) is enhanced with a leaching factor f_l as a simple representation of these processes:

$$C_j = f_l R_{mol}^{j} n_G \tag{14}$$

4 Results & Discussion

The discretised model results and homogenised model results of aperture closure compared with the experimental results are shown in Figure 9 and Figure 10, respectively. The element concentration results from the discretised model (inverse chemistry calculation) and homogenised model (fully coupled geochemistry) compared with the experiment results are shown in Figure 11 and Figure 12, respectively. Consistent with the previous novaculite modelling (Bond *et al.*, 2015; McDermott *et al.*, 2015), both models give a good fit to the hydraulic aperture closure from the granite experiment, but do not reproduce the change in aperture occurring with the change in flow rate. This behaviour is different to the previous study (Bond *et al.*, 2015; McDermott *et al.*, 2015) in which the novaculite experiment exhibited no obvious hydraulic aperture change with changes in flow rate, and it is unclear whether there is a missing process in the models or this feature comes from uncertainty in the control of precise pressure changes within the experiment. The shape and magnitude of the results are used for comparison of the modelled element concentrations to the experiment concentrations, whereby being within a factor of 2 is considered accurate and outside a factor of 10 being inaccurate. This is considered appropriate due to the uncertainties associated with the geochemical parameters (in particular for low temperatures) and to make clear that there is no benefit in fitting the experimental results more precisely. In this regard, the models also give a reasonable fit to the eight element concentrations measured. It should be noted that for the homogenised model only sample ef-3 from the Yasuhara *et al.* (2011) granite experiment has been considered for analysis. This is due to the uncertainties seen in modelling the novaculite experiment (Bond *et al.*, 2015) and the more complex granite geochemistry and variability in the granite experiment data. The ef-3 experiment was selected for having less 'noise' in the measured effluent ion concentrations (Figure 3) and a clear closing trend in the fracture aperture evolution (Figure 4).

The fully coupled geochemistry model used in the homogenised approach (Figure 12) matches the experimental element concentrations quite well for Si, Al, Fe, Ca, Na, Mg with a surface 'roughness' factor of ~7×10^5 but the K concentration is still nearly two orders of magnitude too low. This 'roughness' factor is consistent with modelling the novaculite experiment (Bond *et al.*, 2015) but the physical meaning of increasing the reactive surface area by this amount is difficult to explain solely considering the fracture surface and suggests uncertainty in the micro-scale geometry or a missing process from the model (e.g. subsurface). Further investigation was carried out into rock matrix diffusion in Bond *et al.* (2016c), where it was shown to be a potentially significant source of dissolved ions, although still not sufficient to explain the full required 'roughness' factor and it had no significant impact on the dissolved K. This behaviour is consistent with results for the novaculite, where even 'optimistic' parameterisations of the diffusion process could only fit the observed dissolved silicon concentrations at high temperatures (Neretnieks, 2014; Bond *et al.*, 2015).

The under-prediction of the K concentration in the effluent indicates uncertainty in the geochemical model, possibly through mineral composition or the primary/secondary species in the reactions, or the presence of another unidentified geochemical process. The mineral compositions resulting from the inverse chemistry calculations from Bond *et al.* (2016a), shown in Table 13, are quite different from the composition used in Yasuhara *et al.* (2011) but are more similar to the 'alternative' composition (Table 2). They suggest higher volume percentages of annite and anorthite, and a lower volume percentage orthoclase; the ef-3 inverse calculated composition has a lot less quartz and much more albite than from the literature. This difference is a reflection of the inverse method being fundamentally controlled by the quartz kinetic rates, hence enhancing the proportions of the more minor but faster reacting minerals compensates for the single controlling rate. In this sense, the homogenised and discretised results are in agreement; the geochemical results can only be

understood in terms of the volumetrically disproportionate impact of more reactive minor minerals such as annite.

Further details of the discrete and homogenised granite models and other sensitivity/process investigations are discussed in Bond *et al.* (2016a, 2016c).

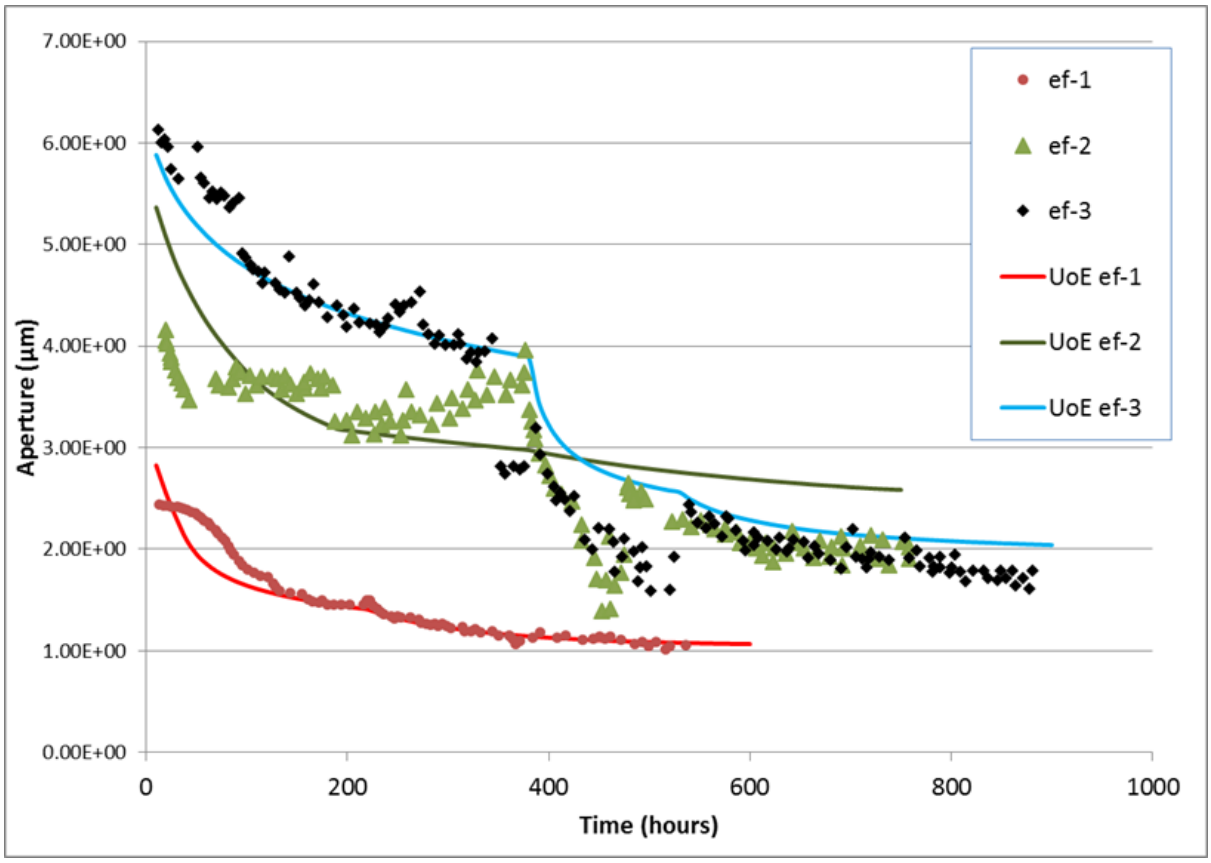

Figure 9: Comparison of modelled aperture closure from discretised model (UoE ef-1, UoE ef-2, UoE ef-3) and experimental aperture closure values (ef-1, ef-2, ef-3) of Yasuhara *et al.* (2011)

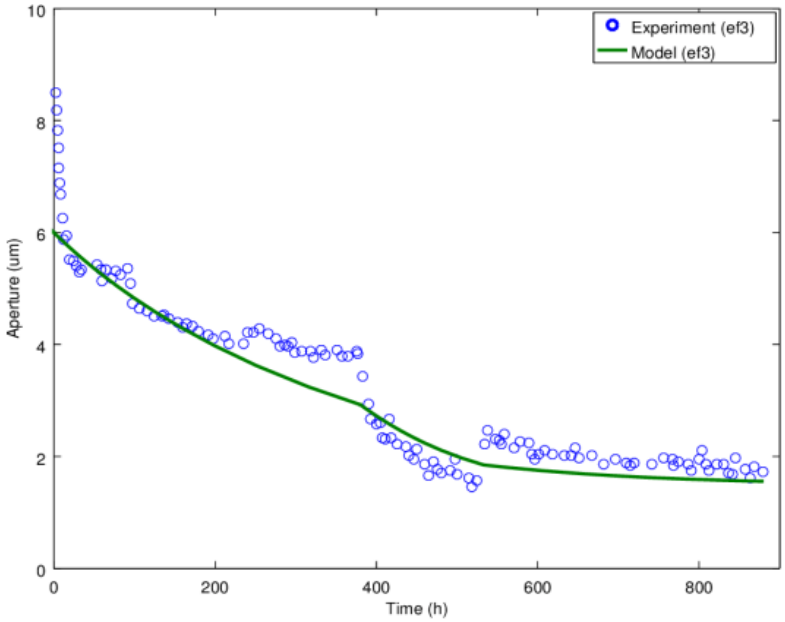

Figure 10: Comparison of modelling aperture closure from homogenised model and experiment aperture closure values (ef-3) of Yasuhara *et al.* (2011)

ef-1

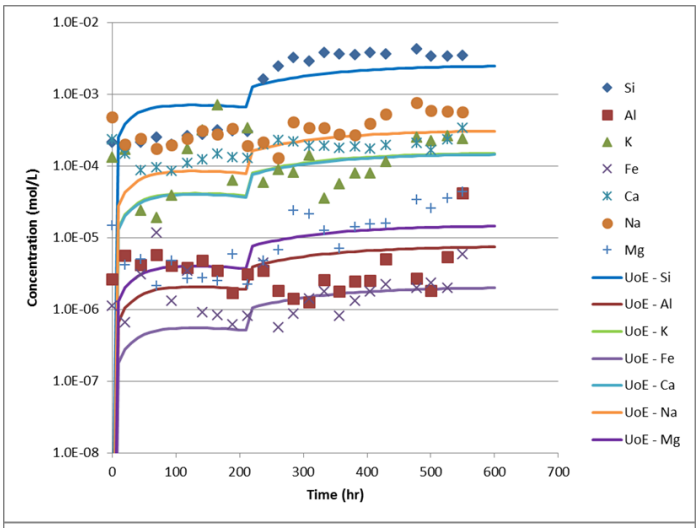

ef-2

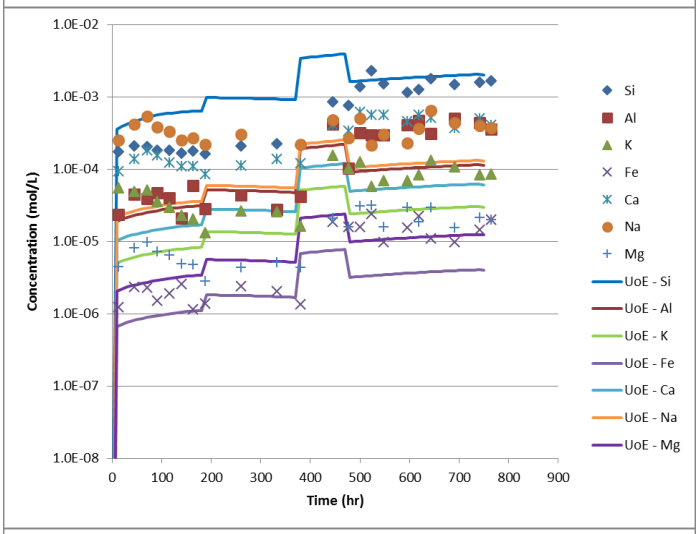

ef-3

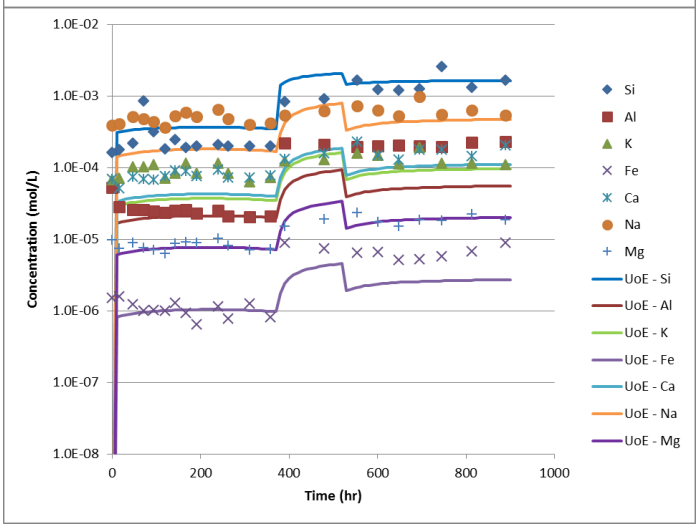

Figure 11: Comparison of modelling element concentration from discretised model inverse concentration calculation (UoE prefix) and experimental element concentration values (no prefix) of Yasuhara *et al.* (2011) for ef-1, ef-2 and ef-3.

Table 13: Granite compositions from inverse concentration calculation used to fit effluent chemistry (from Bond *et al.*, 2016a)

	ef1	ef2	ef3
Volume fractions of quartz and 'granite' (non-quartz)			
Granite (f_G)	70%	70%	90%
Quartz (f_Q)	30%	30%	10%
Leaching Coefficient f_l	15	15	15
Composition of granite going into solution (total percentage in brackets)			
Anorthite	24.64% (17.25%)	28.3% (19.81%)	16.93% (15.237%)
Albite	49.28% (34.50%)	56.5% (39.55%)	67.74% (60.97%)
Orthoclase	24.64% (17.25%)	11.3% (7.91%)	13.55% (12.20%)
Phlogopite	1.23% (0.86%)	2.8% (1.96%)	1.52% (1.37%)
Annite	24.64% (17.25%)	28.3% (19.81%)	16.93% (15.24%)
Al % in solution (f_{Al})	**1.0%**	**40.0%**	**7.0%**

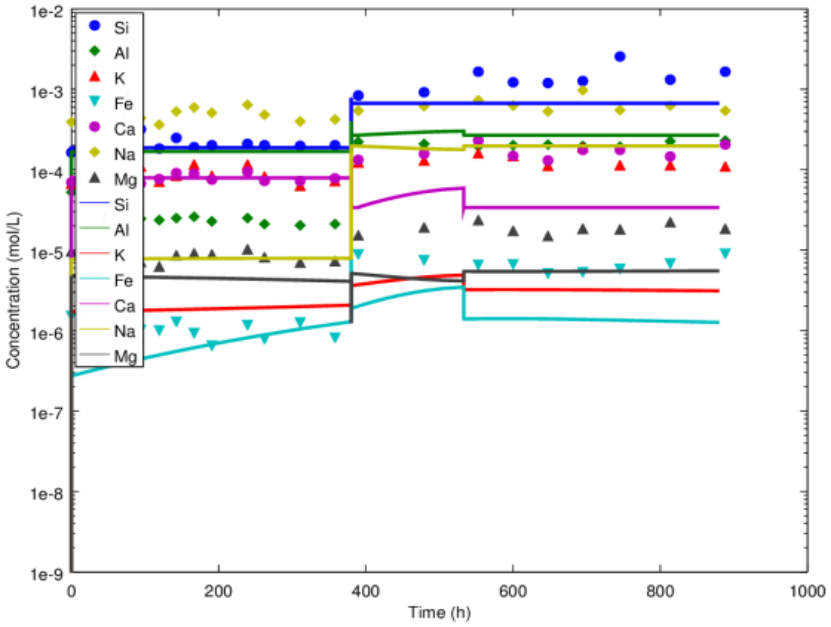

Figure 12: Comparison of modelling element concentration from homogenised model and experimental element concentration values (ef-3) of Yasuhara *et al.* (2011).

The reasonable fits for the experiment hydraulic aperture closure and element concentrations in the discrete and homogenised models from similar input data, give confidence between the two

modelling approaches. However, the degree of calibration and significant process enhancement required in both models highlight the uncertainty in the underpinning processes, limiting the use of the models for blind prediction of evolution of effective fracture transmissivity with the current understanding. This is a general theme across the teams participating in Task C1 of the DECOVALEX project (Bond *et al.*, 2014b, 2016b). However, it is important to clarify that blind prediction of such a small-scale feature is not a necessity and depends on the relevance (e.g. of solute movement in a fractured host rock) in the context of the overall safety case (Galson and Crawford, 2013). It is likely that multiple calibrations of the models could be used to fit the experiment data, but the model results are still representative of the processes in the system. There are also uncertainties between the two modelling approaches; the homogenised model does not currently include any mechanism for representing the channelisation included in the discrete model (seen to be important in the novaculite modelling), and the discrete model does not include a full geochemical model (important for modelling the poly-mineral granite). The geometry of the contacting fracture surface and how it evolves (through change in aperture-contact ratio distribution over time and/or development of preferable flow channels) is a major control for both the discrete and homogenised models, affecting the surface dissolution through the available surface area for reaction on the fracture walls and the stress concentration at contacting asperities for the mechanical closure process (considered as pressure solution in the models), as well as other key processes. Thus, for modelling THMC behaviour of flow through a single fracture in crystalline rock, a good understanding of the fracture geometry is required.

Based on the modelling work presented for both novaculite (Bond *et al.*, 2015; McDermott *et al.*, 2015) and granite (Bond *et al.*, 2016a) experiments, an attempt is made at summarising the key processes, their uncertainties, key controls, and confidence in physical understanding of parameters for modelling THMC behaviour of flow through fractured granite, in Table 14. For this study, the table summarises:

- **Process** – Key process identified in modelling THMC behaviour of flow through fracture granite.
- **Physical Models** – The physical models to consider for simulating the given process.
- **Main Uncertainties** – The main uncertainties to resolve for modelling the given process accurately.
- **Key Process Control** – The main process controls in modelling the given process.
- **Confidence** – The confidence in accurately modelling the given process with the current understanding of the process physical models and uncertainties.
- **Validation** – Evidence that the given process is important.
- **Rank** – Relative importance of modelling the given process on reproducing experimental results; a rank of 1 being most important.

Here, hydraulically driven flow of de-ionised water through the fracture is identified as the most important process to model, since this controls the hydraulic aperture and transport of dissolved ions in the effluent.

The next most important processes for modelling effluent ion concentrations and aperture evolution in the experiment are chemically-driven surface dissolution/precipitation and mechanically-driven aperture closure. Key uncertainties for these processes identified in this study are the fracture geometry affecting both the available reactive surface area and the contact stress concentrations, the kinetic parameters and mineral composition for chemical dissolution, and inability in this study to distinguish between pressure solution / stress corrosion for mechanical closure. It should be

noted here that the mechanically-driven aperture closure only refers to a subset of mechanical closure processes (pressure solution / stress corrosion) that are important to the granite experiment discussed herein, and does not include processes such as mechanical 'creep' of the rock. However, we expect such pure mechanical processes to be very rapid (Matsuki et al., 2001) and indeed, ef-3 shows very rapid early closure that might be interpreted as a pure mechanical response. Furthermore, there is uncertainty over whether the critical stress component considered as a control for mechanically driven aperture closure is actually physical (Neretnieks, 2014) or if it is actually a proxy for other processes which are present in the experiment.

As previously discussed (Bond *et al.*, 2015, 2016a; McDermott *et al.*, 2015), considering these processes alone is not sufficient to fully represent the observed experiment effluent ion concentrations and aperture evolution (novaculite experiment). Rock matrix diffusion and channelization processes, respectively, are considered next most important to model the experiment though there is uncertainty over their parameterisation. It is unclear whether full representation of these processes is required or whether there are alternate approaches which can be used to provide an appropriate level of approximation.

Finally, elastic fracture opening and closing due to change in induced strain on the rock is not considered important for the experiment stresses. However, there is potential for this process to become important when considering flow through rock fractures under larger stress.

Although not identified as a separate process in Table 14, a main uncertainty underpinning all the identified processes is the appropriate representation of the fracture geometry.

Table 14: Summary of key processes and their uncertainties considered for modelling THMC behaviour in flow through fractured granite

Process	Physical Models	Main Uncertainties	Key Process Control	Confidence	Validation	Rank
Hydraulically driven flow of de-ionised water through fracture	Darcy flow Fluid properties Fracture geometry	Scale and resolution of fracture aperture Application of cubic law	Pressure gradient Aperture spacing and distribution	Local scale flow approximated. At higher pressure gradients the viscous flow approximation breaks down. Validity of cubic law using up-scaled approach in homogenised model	Measured hydraulic pressure and measured flow rate through fracture Hydraulic and mechanical aperture are consistent	1
Chemically driven surface dissolution (and precipitation)	Kinetically controlled reactive transport	Fracture surface 'roughness' Heterogeneity (3D) of minerals available for reaction on the surface (granite) Kinetic parameters Formation of complexants and secondary minerals	Temperature Concentration of aqueous species Reaction rates Hydraulic flow rate	Uncertainty of the physical meaning of large surface area enhancements required Lack of information about multiple micro-scale geometry and interaction with physical processes	Change of hydraulic aperture reflecting change in mechanical aperture Effluent concentration of aqueous species (mass balance) Evolution of effective surface area	2
Mechanically driven aperture closure	Pressure solution Stress corrosion	Scale and resolution of fracture aperture Geometry of contacting fracture surfaces Inability to distinguish between main process sets	Stress concentration at contact areas Increase in contact surface area due to pressure solution Critical stress below which no pressure solution possible The hardest mineral in the rock, quartz, exerts a significant control in pressure solution dominated systems	Pressure solution requires significant enhancement for modelling both novaculite and granite experiments Geometrical approximations required Modelling these processes for poly-mineral rock not fully understood	Change of hydraulic aperture reflecting change in mechanical aperture Effluent concentration of aqueous species (mass balance) Clear non-linear relationship in the rate of change of mechanical aperture related to the rate of change of confining stress	2
Rock matrix diffusion	Diffusion of chemical species between fracture and rock matrix adjacent to the fracture	Extent of accessible volume of matrix for geochemical exchange.	Concentration of aqueous species Relative size of surface area and accessible volume available for ion diffusion Pore connectivity	Phenomenology of RMD process well-understood Measurement of parameters difficult.	Effluent concentration of aqueous species	3
Channelisation	Fluid flow Localised surface dissolution	Location of channels Number and size of channels	Dissolution of smallest channel bridges in fracture surface Kinetic driven dissolution	Sub-measurement resolution scale feature. Parameters approximate process known to occur, but no validation Empirical fitting	Change of hydraulic aperture reflecting change in mechanical aperture Mass transport characteristics	3
Elastic fracture closure and opening	Rock stress and fluid pressure induced strain	Aperture geometry Contact stress Fluid pressure	Elastic properties of rock minerals	Numerical and empirical models allow reasonable approximation of elastic strain	Change of hydraulic aperture reflecting change in mechanical aperture	4

5 Conclusions

Discretised and homogenised coupled process models have been developed and separately calibrated then benchmarked against one another, and subsequently used to identify the relative importance and uncertainty of different T, H, M, C processes in the context of this Task and the related dataset when modelling flow through fractured granite. These results provide insight into the importance of different processes operating during flow and transport through fractured rock.

Both the discretised and homogenised coupled processes modelling approaches have been shown to produce similar results when using very similar input data. This demonstrates the possibility of being able to use homogenised approaches, potentially underpinned by discretised approaches, to represent multiple features rather than be limited to single fracture representations. Uncertainty about the processes in both models limit their use for prediction. In particular, there is uncertainty over whether stress corrosion or pressure solution is the dominant closure mechanism and over the significance of rock matrix diffusion in the granite experiment. This is highlighted by the degree of calibration that was required for both models, including significant enhancement of both the pressure solution and surface dissolution processes. These results from modelling the Yasuhara *et al*. (2011) granite experiment are consistent with the modelling of the Yasuhara *et al*. (2006) novaculite experiment (McDermott *et al.*, 2015; Bond *et al.*, 2015).

A summary of the different processes modelled during fluid flow through a fractured sample, and a ranking of the impact of these processes on the overall flow behaviour is presented in Table 14. The selection of the geometrical profile of the fracture surfaces was shown to have a significant control on the rate and impact of the various processes modelled. Although there is uncertainty in the geometrical profile, the impact of the effect of the controlling processes can still be used to determine their relative importance.

References

Aagaard, P. and Helgeson, H.C. (1982). Thermodynamic and kinetic constraints on reaction rates among minerals and aqueous solutions. I. Theoretical considerations, American Journal of Science 282 (3), 237–285.

Andra (2014). ThermoChimie thermodynamic database version 9 (dated from January 2014). https://www.thermochimie-tdb.com/

Benbow SJ, Rivett MO, Chittenden N, Herbert AW, Watson S, Williams SJ and S Norris (2014) Potential migration of buoyant LNAPL from Intermediate Level Waste (ILW) emplaced in a geological disposal facility (GDF) for UK radioactive waste. Journal of Contaminant Hydrology 167, 1–22

Bernier, F., Li, X., Bastiaens, W., Ortiz, L., Van Geet, M., Wouters, L., Frieg, B., Blumling, P., Desrues, J., and Viaggiani, G., Bühler Ch.(2007) Fractures and self-healing within the excavation disturbed zone in clays (Selfrac), Final report, 5th EURATOM Framework Programme (1998–2002).

Bethke, C.M. (2008). Geochemical and Biogeochemical Reaction Modeling. Cambridge University Press.

Bond A.E., Egan M.J., Metcalfe R.C., Robinson P.C. and Towler G. (2010). Understanding controls on the performance of engineered barrier systems in repositories for high-level radioactive waste and

spent fuel. UK Environment Agency Report SC060055. https://www.gov.uk/government/uploads/system/uploads/attachment_data/file/291238/scho0910bsze-e-e.pdf

Bond A, Millard A, Nakama S, Zhang C, Garitte B. (2013) Approaches for representing hydromechanical coupling between large engineered voids and argillaceous porous media at ventilation experiment, Mont Terri. Journal of Rock Mechanics and Geotechnical Engineering 2013; 5 (2).

Bond, A., Thatcher, K., Chittenden, N., McDermott, C., and Fraser-Harris, A. (2014a). RWM Coupled Processes Project: First Annual Report for RWM participation in DECOVALEX-2015 Tasks A and C1. Externally peer reviewed AMEC report 18040-TR-002 v2.1. https://rwm.nda.gov.uk/publication/rwm-coupled-processes-project-first-annual-report-for-rwm-participation-in-decovalex-2015-tasks-a-and-c1/

Bond, A.E., Chittenden, N., Fedors, R., Lang, P.S., McDermott, C.I., Neretniecks, I., Pan, P.Z., Sembera, J., Watanabe, N. and Yasuhara, H., (2014b). Coupled THMC modelling of a single fracture in novaculite for DECOVALEX-2015. Proceedings of DFNE 2014, 1st International Conference on Discrete Fracture Network Engineering (Vancouver) October 2014.

Bond, A., Thatcher, K., Chittenden, N., McDermott, C. and Fraser-Harris, A. (2015). RWM Coupled Processes Project: Second Annual Report for RWM participation in DECOVALEX-2015 Tasks A and C1. Externally peer reviewed AMEC report 18040-TR-003 v3.0. https://rwm.nda.gov.uk/publication/rwm-coupled-processes-project-second-annual-report-for-rwm-participation-in-decovalex-2015-tasks-a-and-c1/

Bond, A., Thatcher, K., Chittenden, N., McDermott, C. and Fraser-Harris, A. (2016a). RWM Coupled Processes Project: Third Annual Report for RWM participation in DECOVALEX-2015 Tasks A and C1. Externally peer reviewed AMEC report 18040-TR-004 v2.0. https://rwm.nda.gov.uk/publication/rwm-coupled-processes-project-third-annual-report-for-rwm-participation-in-decovalex-2015-tasks-a-and-c1/

Bond, A., Pan, P.Z., Feng, X.T., Zheng, H., Fedors, R., Gwo, J.P., Cao, T., Lang, P., Neretnieks, I., Chittenden, N., Šembera, J., Brusky, I., McDermott, C. and Watanable, N. (2016b). DECOVALEX-2015 Task C1 Final Report. *In press*.

Bond, A., Thatcher, K., Chittenden, N., McDermott, C., Fraser-Harris, A. and Wilson J. (2016c). Final Report of the Coupled Processes Project: Outcomes from DECOVALEX-2015. Externally peer reviewed AMEC report 18040-TR-005 v1.0. https://rwm.nda.gov.uk/publication/final-report-of-the-coupled-processes-project-outcomes-from-decovalex-2015/

BRGM (2011). Thermoddem geochemical database, Geochemist's Workbench version 'gwb_lv1_thermoddem_lvl1_no-org_15dec11'. http://thermoddem.brgm.fr/recherche.asp

Galson, D. A., and Crawford, M. B. (2013). Treatment of Coupled Processes in Geological Disposal: Review of UK Work, and Treatment of Coupled Processes in Performance Assessments in other Countries. Externally peer reviewed AMEC report 18040-TR-001 v1.0. https://rwm.nda.gov.uk/publication/treatment-of-coupled-processes-in-geological-disposal-review-of-uk-work-and-treatment-of-coupled-processes-in-performance-assessments-in-other-countries/

Garven, G., Manning, C. E. and Yardley, B. W. D. (2010), Frontiers in geofluids: editorial. Geofluids, 10: 1–2. doi:10.1111/j.1468-8123.2010.00290.x

Goodwin, L. B., Mozley, P. S., Moore, J. C., and Haneberg, W. C., 2013, Introduction, Faults and Subsurface Fluid Flow in the Shallow Crust, American Geophysical Union, p. 1-5.

Harlov, D., Austrheim, H. (Eds.), (2013). Metasomatism and the chemical transformation of rock: The role of fluids in terrestrial and extraterrestrial processes, (Lecture Notes in Earth System Sciences), Springer,pp 806, ISBN: 978-3-642-28393-2

JNC (2000). Regional Hydrogeological Study Project Results from 1992-1999 Period. JNC Technical Report, JNC TN7400 2000-014 (in Japanese with English abstract).

Kolditz O (1997). Strömung, Stoff- und Wärmetransport im Kluftgestein, Berlin-Stuttgart, Borntraeger Verlag.

Kolditz, O., Görke, U.-J., Shao, H., Wang, W., Bauer, S. (Eds.) (2016): Thermo-Hydro-Mechanical-Chemical Processes in Fractured Porous Media: Modelling and Benchmarking - Benchmarking Initiatives. Springer Publisher, ISBN 978-3-319-29224-3.
http://www.springer.com/gp/book/9783319292236

Matsuki, K., Wang, E. Q., Sakaguchi, K., & Okumura, K. (2001). Time-dependent closure of a fracture with rough surfaces under constant normal stress. International Journal of Rock Mechanics and Mining Sciences, 38(5), 607–619.

Maul, P., (2013). QPAC: Quintessa's general-purpose modelling software. Quintessa Report QRS-QPAC-11. Available at www.quintessa.org

McDermott, C., Bond, A., Fraser-Harris, A., Chittenden, N. and Thatcher, K. (2015). Application of hybrid numerical and analytical solutions for the simulation of coupled thermal hydraulic mechanical and chemical processes during fluid flow through a fractured rock. Environmental Earth Sciences, Thematic Issue, DOI: 10.1007/s12665-015-4422-7.

Neretnieks, I. (2014). Stress-mediated closing of fractures – Impact of matrix diffusion. Journal of Geophysical Research Solid Earth, 119 (5), 4149-4163.

Ouyang T, Tamma KK, (1996) ON adaptive time stepping approaches for thermal solidification processes. International Journal of Numerical Methods for Heat and Fluid Flow, v. 6, no. 2, p. 37-50.

Palandri, J.L. and Kharaka, Y.K. (2004) A compilation of rate parameters of mineral-water interaction kinetics for application to geochemical modeling. US Geological Survey Open File Report 2004-1068. USA.

Wang W, Görke UJ, Kolditz O, (2011a) Adaptive time stepping with automatic control for modeling nonlinear H2M coupled processes in porous media. 45th US Rock Mechanics / Geomechanics Symposium. 30

Wang W, Schnicke T, Kolditz O, (2011b) Parallel finite element method and time stepping control for non-isothermal poro-elastic problems. Computers, Materials and Continua, v. 21, no. 3, p. 217-235.

Yasuhara, H., Polak, A., Mitani, Y., Grader, A.S., Halleck, P.M. and Elsworth, D. (2006). Evolution of fracture permeability through fluid-rock reaction under hydrothermal conditions. Earth and Planetary Science Letters 244, 186–200.

Yasuhara, H., Kinoshita, N., Ohfuji, H., Lee, D.S., Nakashima, S., and K. Kishida. (2011). Temporal alteration of fracture permeability in granite under hydrothermal conditions and its interpretation by coupled chemo-mechanical model. Applied Geochemistry 26: 2074–2088.

Yuguchi, T., Tsuruta, T. and Nishiyama, T. (2010). Zoning of rock facies and chemical composition in the Toki granitic body, Central Japan. Japanese Magazine of Mineralogical and Petrological Sciences 39 (2), 50-70.